Chinese Chemical Letters 37 (2026) 112530

Contents lists available at ScienceDirect

Chinese Chemical Letters

journal homepage: www.elsevier.com/locate/cclet

Dual-identification strategy for global profiling of protein fatty acylation sites

Pengfei Wu, Chang Sun, Xiao Huang, Wenjing Nie, Qiongqiong Wan, Qingtao Meng*, Suming Chen*

The Institute for Advanced Studies, Renmin Hospital of Wuhan University, Wuhan University, Wuhan 430072, China

ARTICLE INFO

Article history:
Received 28 October 2025
Revised 23 January 2026
Accepted 13 February 2026
Available online 14 February 2026

Keywords:
Fatty acylation
Mass spectrometry
Metabolic labeling
Click chemistry
Palmitoylation

ABSTRACT

Protein fatty acylation encompasses S/N/O-acylation modifications that regulate diverse cellular functions, yet current methods cannot simultaneously capture all three types. Here, we present a dual-identification strategy that integrates metabolic labeling with click chemistry, hydroxylamine mediated selective hydrolysis, and cleavable bioorthogonal probes for comprehensive fatty acylation site detection. Using Alk-C16:0 and Alk-C18:0 probes in HepG2 cells, we identified 1310 and 1131 total fatty acylation sites respectively, including 588 and 674 S-acylation sites substantially exceeding single method coverage. Integration of open and closed searches revealed probe intracellular conversion induced acyl chain heterogeneity, improving identification accuracy. We discovered diagnostic ions revealing acyl chain structure and N-acylation specific cyclic immonium ions that discriminate between modification subtypes. This strategy enables unprecedented comprehensive protein fatty acylation characterization, providing a robust platform for investigating molecular mechanisms of these essential modifications.

© 2026 Published by Elsevier B.V. on behalf of Chinese Chemical Society and Institute of Materia Medica, Chinese Academy of Medical Sciences.

Protein fatty acylation, as a subset of lipidation represents a fundamental class of posttranslational modifications (PTMs). wherein long chain fatty acids form covalent bonds with proteins, thereby modulating protein activity, subcellular localization, and stability while playing pivotal roles in cellular signaling, membrane protein targeting, and cellular homeostasis [1–4]. The major types of fatty acylation include S-acylation, N-acylation, and O-acylation. S-Acylation constitutes a reversible modification typically involving palmitic acid covalently linked to cysteine residues through thioester bonds, regulated by the coordinated action of palmitoyltransferases and acyl protein thioesterases [5]. Palmitoylation, the most extensively studied fatty acylation type, plays critical roles in neuroinflammation, cancer, and Parkinson's disease progression [6–9]. N-Acylation involves fatty acid attachment to specific amino acid residues *via* amide bonds, with N-myristoylation being the most prevalent form, catalyzed by N-myristoyltransferase (NMT) that links myristate to N-terminal glycine residues through amide bonds. Recent investigations have revealed that N-acylation can also occur on lysine residues [10,11]. O-acylation encompasses fatty acid attachment to serine or threonine residues *via* oxygen ester linkages, with porcupine implicated in Wnt Ser209 O-acylation and lysophosphatidylcholine acyltransferase I (Lpcat1) catalyzing histone O-palmitoylation [12,13]. Despite limited research on N/O-acylation, these modifications exert indispensable functions in protein secretion, maturation, and subcellular localization.

The identification of fatty acylation modification sites is instrumental in elucidating their molecular mechanisms and provides critical support for disease diagnostics and therapeutic target development. The absence of specific antibodies renders large-scale fatty acylation identification challenging [2,14]. Current identification approaches encompass two major categories: Endogenous palmitate mediated palmitoylation site identification and click chemistry based metabolic labeling methodologies. Endogenous palmitoylation identification methods include acyl-RAC (resin-assisted capture) [15] and the recently developed nanographene fluoride solid-phase extraction [16], with their primary limitations being false positives arising from incomplete thiol blocking and exclusive applicability to S-acylation sites. Click chemistry based metabolic labeling employs fatty acid analog probes bearing alkyne or azide groups for protein incorporation, followed by click chemistry mediated conjugation with biotin for efficient protein modified by fatty acid enrichment or with fluorophores for protein visualization [17,18]. Combined with hydroxylamine mediated selective hydrolysis and thiol specific blocking, this approach enables S-acylation site identification [10,19–21]. However, the loss of acyl chain information precludes analysis of lipidated protein

* Corresponding authors.
E-mail addresses: qtmeng@whu.edu.cn (Q. Meng), sm.chen@whu.edu.cn (S. Chen).

https://doi.org/10.1016/j.cclet.2026.112530
1001-8417/© 2026 Published by Elsevier B.V. on behalf of Chinese Chemical Society and Institute of Materia Medica, Chinese Academy of Medical Sciences.

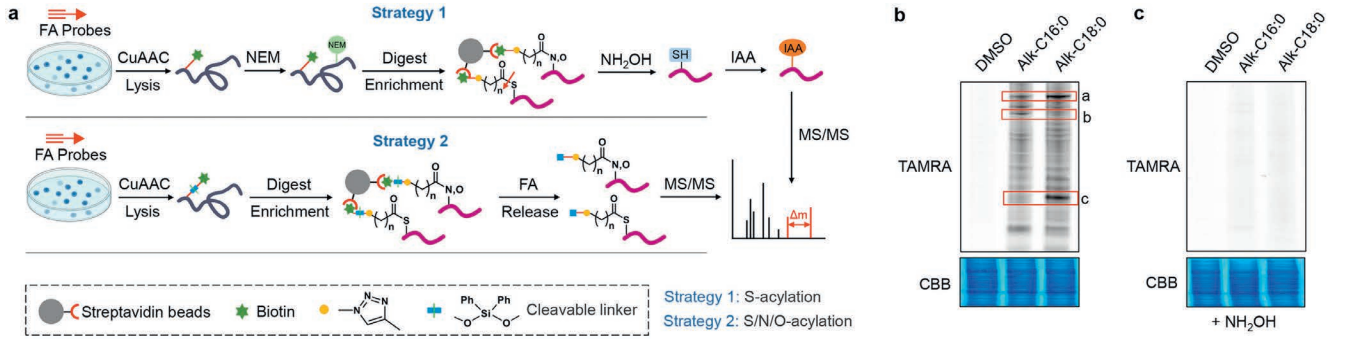


Fig. 1. Chemical proteomics strategy based on metabolic labeling for identifying fatty acylation sites. (a) Workflow of dual-identification strategies. (b) SDS-PAGE analysis of proteins labelled with fatty acid probes was performed by incubating HepG2 cells with 30 μmol/L Alk-C16:0 or Alk-C18:0 probes for 12 h, subjecting cell lysates to CuAAC with TAMRA-azide, and analyzing by in-gel fluorescence to detect probe-labeled proteins. (c) In-gel fluorescence analysis post-hydroxylamine treatment.

acyl chain heterogeneity. Metabolic labeling coupled with cleavable bioorthogonal tags efficiently releases lipidated peptides, enabling tandem mass spectrometry based identification of fatty acylation sites with intact acyl chains [22]. Nevertheless, thioester instability leads to metabolic tag loss during sample preparation and tandem mass spectrometry analysis, potentially impeding large scale identification. Consequently, these two metabolic labeling approaches offer complementary advantages: The former achieves efficient S-acylation identification while the latter excels in acyl chain heterogeneity analysis. Although studies have demonstrated the existence of substantial N/O-acylated proteins [10], methodologies for large-scale N/O-acylation site identification remain to be developed.

In this study, we established a dual-identification strategy that leverages the complementary advantages of hydroxylamine mediated selective hydrolysis and cleavable bioorthogonal tags within a click chemistry based metabolic labeling framework, enabling comprehensive identification of S/N/O-acylation modifications. Initially, we optimized the sample processing workflow and LC-MS/MS analytical conditions for the cleavable bioorthogonal tag approach, implementing an integrated open and closed search data analysis strategy for result interpretation that revealed probe metabolism induced acyl chain heterogeneity. Furthermore, through systematic diagnostic ion mining, we elucidated the fragmentation patterns of lipidated peptides in tandem MS: S/N/O-acylation modifications generate characteristic diagnostic ions with Δm values exhibiting systematic variation correlating with acyl chain length and saturation; N-acylation modification spectra characteristically display diagnostic ions paired with cyclic immonium ions. These signature diagnostic ions not only effectively indicate acyl chain heterogeneity in fatty acylation modifications but also enhance the confidence of modification type discrimination. Finally, we employed Alk-C16:0 and Alk-C18:0 probes to identify fatty acylation sites in HepG2 cells, comparing the differential distribution patterns and modification types of fatty acids with varying chain lengths, while analyzing functional disparities among the corresponding modified proteins. This methodology provides a powerful tool for in-depth elucidation of fatty acylation modification molecular mechanisms.

The detailed experimental methods including cell culture, metabolic labeling, in-gel fluorescence analysis, identification of fatty acylation sites using cleavable bioorthogonal labeling, identification of fatty acylation sites by NH_2OH mediated selective hydrolysis and thiol specific blocking, LC-MS analysis, and data analysis were described in Supporting information.

To achieve efficient identification of S/N/O-acylation, we established a dual-identification strategy (Fig. 1a). Strategy 1 integrates hydroxylamine mediated selective hydrolysis with thiol specific blocking. The workflow proceeds as follows: Following probe incubation, azide modified biotin is added to the protein lysate for CuAAC reaction with alkyne containing protein modified by fatty acid; free sulfhydryl groups are subsequently blocked using *N*-ethylmaleimide (NEM), followed by labeled protein enrichment and enzymatic digestion; neutral hydroxylamine is then employed to selectively hydrolyze thioester bonds, with iodoacetamide (IAA) blocking newly exposed sulfhydryl groups, thereby introducing specific mass tags at S-acylation sites for ultimate identification *via* mass spectrometry-based proteomics. Strategy 2 employs acid cleavable azide modified biotin for CuAAC, enabling efficient release of enriched lipidated peptides from streptavidin-modified agarose beads through formic acid treatment, thereby simultaneously elucidating acyl chain structure, modification sites, and modification types.

To investigate the differential modification sites of probes with varying carbon chain lengths and their impact on acyl chain heterogeneity, we employed Alk-C16:0 alongside the widely utilized palmitoylation probe Alk-C18:0 (Fig. S1a in Supporting information). Given that the liver serves as the principal organ for lipid metabolism and the primary site of fatty acid biosynthesis in humans, we selected the extensively characterized hepatocellular carcinoma cell line HepG2 as our cellular model system [23]. Target proteins were conjugated to carboxytetramethylrhodamine (TAMRA) *via* copper-catalyzed azide-alkyne cycloaddition (CuAAC) utilizing the terminal alkyne moiety of the probes. SDS-PAGE fluorescence analysis and cell viability assays demonstrated that 30 μmol/L is a safe concentration for both probes to achieve optimal labeling efficiency in HepG2 cells (Fig. 1b and Fig. S2 in Supporting information). However, exhibited distinct modification patterns across different molecular weight ranges. Specifically, Alk-C18:0 demonstrated higher modification abundance than Alk-C16:0 in regions a and c, while the converse was observed in region b (Fig. 1b). Neutral hydroxylamine, which hydrolyzes thioester bonds, serves as a diagnostic reagent for S-acylation detection. Treatment with hydroxylamine resulted in substantial reduction of fluorescence intensity for both probes, indicating that S-acylation constituted the predominant modification type over other acyl modifications (Fig. 1c).

To address the methodological gap in identifying S/N/O-acylation modification sites through metabolic labeling combined with cleavable bioorthogonal tagging, we developed and optimized a cleavable bioorthogonal labeling approach. During sample preparation, the inherent instability of thioester bonds poses a risk of acyl chain loss, particularly when dithiothreitol (DTT) is employed as the reducing agent during reductive alkylation, where acyl chain loss rates are substantially higher compared to tris(2-carboxyethyl)phosphine (TCEP) [24,25]. Consequently, we selected TCEP as the reducing agent for this study. To achieve complete peptide release from streptavidin beads under mild conditions, we

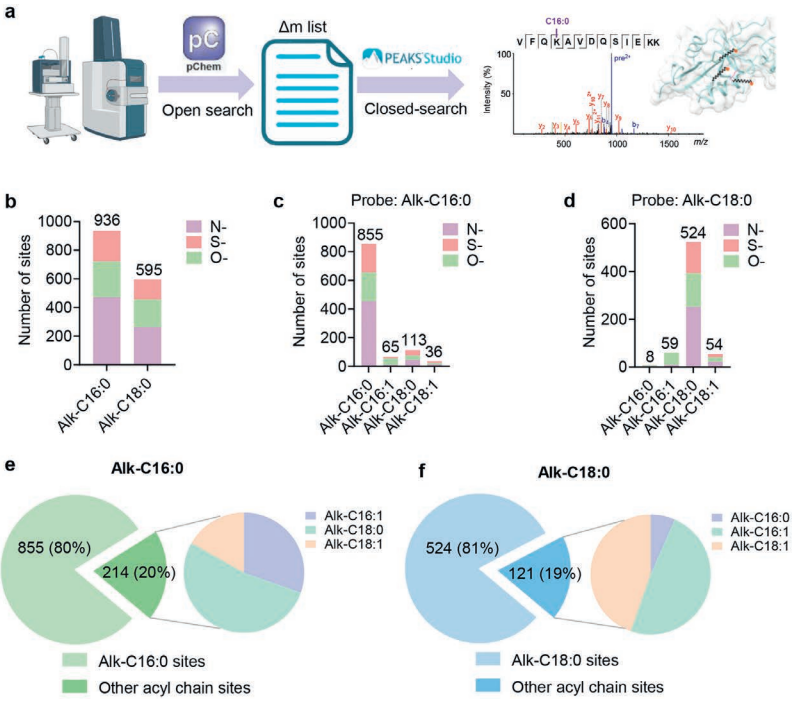


Fig. 2. Cleavable bioorthogonal probes for acylation site identification. (a) Workflow for data analysis in lipid acylation site identification. (b) Comparison of acylation site counts identified by two fatty acid probes. (c, d) Analyses of acyl chain heterogeneity and acylation types at sites detected by Alk-C16:0 and Alk-C18:0 probes (FDR = 0.01, Ascore = 20, $n = 3$ independent biological replicates), The final dataset was generated by combining the union of sites identified in any of the three replicates, followed by removal of sites detected in control samples to maximize coverage. (e, f) Proportional distributions of distinct acyl chain compositions at acylation sites detected by Alk-C16:0 and Alk-C18:0 probes.

utilized the acid-cleavable probe azide-DADPS-biotin (Fig. S1b in Supporting information) [26]. Previous investigations have demonstrated that S-acylated peptides remain stable in 10 % formic acid solution for 2 h [22]. To minimize non-specific hydrolysis of acyl chains during acid cleavage, we reduced both the formic acid concentration and incubation time. Through hydrolysis of azide-DADPS-biotin, we found that 3 % FA for 30 min was sufficient to completely cleave the acid labile groups (Figs. S3 and S4 in Supporting information). We further compared the fatty acylation sites identified using 3 % FA for 30 min *versus* 10 % FA for 60 min. The results showed that while the total number of fatty acylation sites identified was comparable, the 3 % FA 30 min condition yielded a higher number of S-acylation sites while also reducing experimental time (Fig. S5 in Supporting information). Accordingly, we selected 3 % FA for 30 min as our final elution condition. Given the low abundance and high hydrophobicity of lipidated peptides, conventional proteomic strategies prove inadequate. Therefore, we systematically optimized the peptide dissolution system, liquid chromatography (LC) elution gradient, and collision-induced dissociation (CID) fragmentation energy. To enhance lipidated peptide solubility, we evaluated formic acid solutions with varying acetonitrile concentrations as dissolution systems, identifying 40 % acetonitrile as optimal for maximizing fatty acylation site identification (Fig. S6a in Supporting information). Similarly, we optimized the LC elution gradient by testing initial acetonitrile concentrations ranging from 30 % to 50 %. Results demonstrated a progressive decline in fatty acylation site identification with increasing acetonitrile concentrations (Figs. S6b and c in Supporting information). However, initial acetonitrile concentrations below 30 % frequently caused column clogging; consequently, 30 % acetonitrile was determined to be the optimal initial elution concentration. Although we attempted to optimize collision energy to minimize acyl chain loss during secondary fragmentation, decreasing collision energy resulted in substantial reduction of overall fatty acylation site identification (Fig. S6d in Supporting information). This phenomenon likely stems from incomplete precursor ion fragmentation at lower collision energies, leading to reduced b/y ion abundance and compromised peptide identification. These comprehensive optimizations significantly enhanced the identification of S/N/O-acylation sites, providing robust technical support for comprehensive characterization of complex fatty acylation.

We established a comprehensive data analysis pipeline for cleavable bioorthogonal labeling using metabolic labeling coupled with cleavable bioorthogonal tagging technology to identify S/N/O-acylation sites for Alk-C16:0 and Alk-C18:0 in HepG2 cells (Fig. 2a). Liquid chromatography-tandem mass spectrometry (LC-MS/MS) analysis was performed using trapped ion mobility spectrometry (TIMS). To investigate acyl chain heterogeneity, we conducted open searches on raw data using pChem [27], revealing that Alk-C16:0 ($\Delta m = 377.30$) modifies both cysteine and lysine residues, where cysteine modifications likely represent S-acylation while lysine modifications correspond to Nε-Lys-fatty-acylation. Additionally, we observed that the fatty acid probes undergo intracellular conversion, including conversion of Alk-C16:0 to Alk-C16:1 ($\Delta m = 375.28$) and Alk-C18:0 ($\Delta m = 405.33$) modifications on lysine residues (Tables S1 and S2 in Supporting information). Similarly, Alk-C18:0 modified both cysteine and lysine residues, with converted forms including Alk-C16:0 modifications on cysteine (Table S3 in Supporting information). Consequently, our mass shift (Δm) list for subsequent closed searches using PEAKS Studio [28] encompassed Alk-C16:0, Alk-C18:0, and their desaturated forms Alk-C16:1 and Alk-C18:1. This analytical framework enabled identification of 936 modification sites using Alk-C16:0, with N-acylation representing the predominant modification type. Alk-C18:0 identified 595 modification sites, with N-acylation similarly constituting the major modification class (Fig. 2b). Acyl chain heterogeneity analysis revealed that Alk-C16:0 probe derived modifications retained approximately 80 % of the original Alk-C16:0 structure,

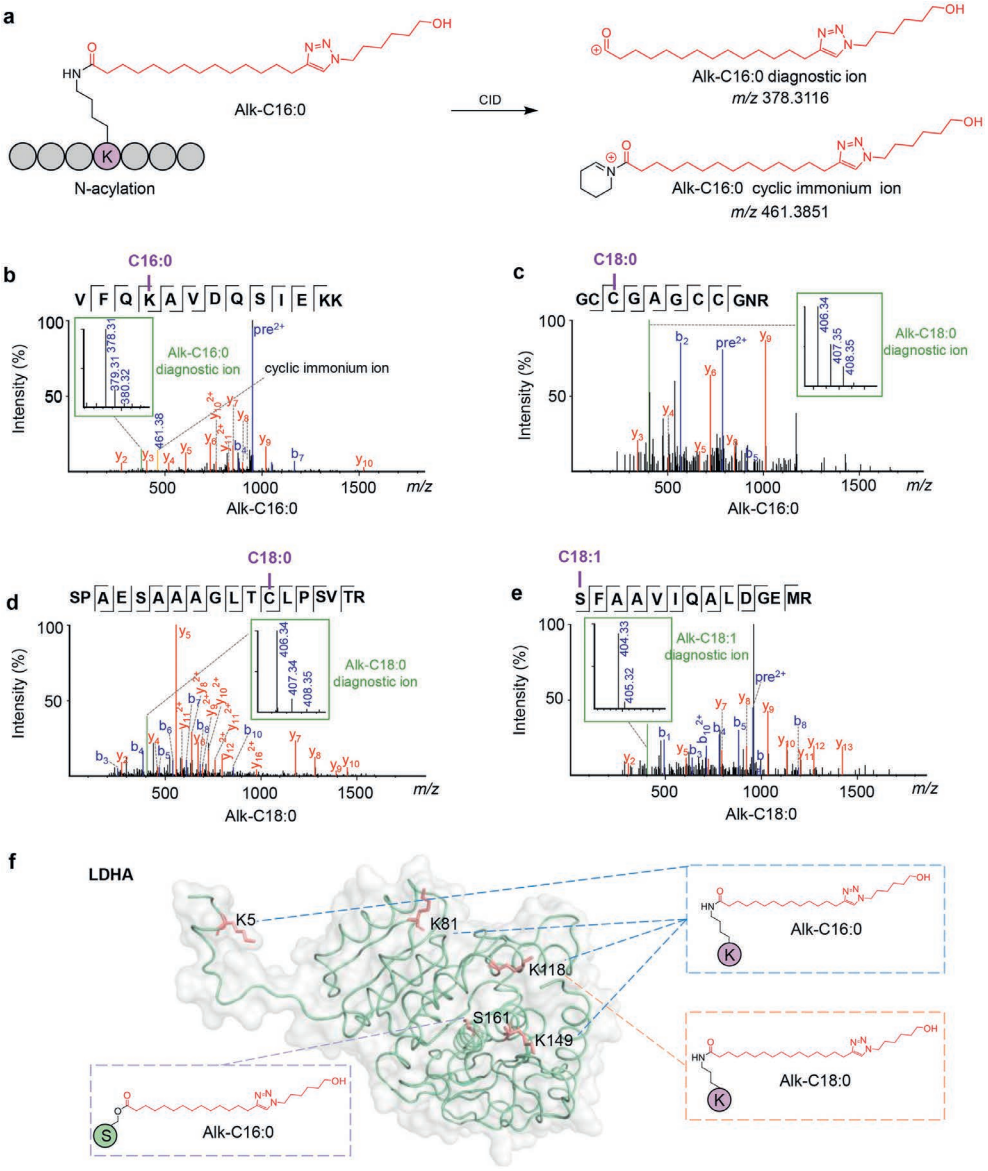


Fig. 3. Diagnostic ion mining from MS/MS spectra of acylated peptides. (a) Two diagnostic ions generated by CID of Alk-C16:0 covalently linked *via* an amide bond to a lysine residue of the peptide. Tandem mass spectra of acylated peptides identified using the Alk-C16:0 probe: (b) Alk-C16:0 modification at K31 of SCRB2, (c) Alk-C18:0 modification at C75 of T4S5. Tandem mass spectra of acylated peptides identified using the Alk-C18:0 probe: (d) Alk-C18:0 modification at C67 of SFT2C, (e) Alk-C18:1 modification at S53 of FDFT. (f) Fatty acylation profile of LDHA.

while ~20% comprised conversion derivatives, predominantly Alk-C18:0 forms (Figs. 2c and e, Table S4 in Supporting information). For Alk-C18:0 probe derived modifications, ~81% maintained the original Alk-C18:0 structure, with ~19% representing conversion derivatives, primarily Alk-C18:1 and Alk-C16:1 forms (Figs. 2d and f, Table S5 in Supporting information). Previous investigations employing azide-terminated fatty acid probes coupled with quantitative analysis of acyl-CoA changes revealed similar probe conversion behaviors [29]. Through integrated open and closed search strategies, we elucidated fatty acid probe heterogeneity arising from intracellular conversion at the protein fatty acylation level, achieving enhanced precision in protein fatty acylation identification.

The introduction of modification specific diagnostic ions for PTMs significantly enhances the confidence of modified peptide identification [30–32]. Previous studies have reported that y-type ions in palmitoylated peptides frequently exhibit palmitate loss under CID and higher-energy collisional dissociation (HCD) conditions [25]; however, diagnostic ions specific to fatty acylation modifications remain uncharacterized. To fill this gap, we systematically investigated diagnostic ions specific to fatty acylation modifications and their fragmentation behavior in tandem mass spectrometry spectra. Through analysis of the low mass region in tandem mass spectra of Alk-C16:0 acyl chains, we identified a characteristic ion at *m/z* 378.31 present across all S/N/O-acylation modifications, enabling preliminary structural elucidation (Figs. 3a and b, Fig. S7 in Supporting information). Remarkably, this diagnostic ion varies with acyl chain heterogeneity. Chain elongation of Alk-C16:0 to Alk-C18:0 correspondingly shifts the diagnostic ion to *m/z* 406.34 (Fig. 3c and Fig. S8 in Supporting information). Additionally, we noted that lysine acylation modifications such as itaconylation and lactylation typically generate cyclic immonium ions under CID and HCD conditions [31,33,34]. Manual inspection revealed similar cyclic immonium ions in N-acylation modification spectra, which also vary with acyl heterogeneity. For instance, following chain elongation of the Alk-C16:0 probe and subsequent modification of K8 on FUT6, the paired diagnostic ions shift to

m/z 406.34 and *m/z* 489.41, respectively (Figs. 3a and b, Fig. S9 in Supporting information). Notably, cyclic immonium ions were absent in O-acylation and S-acylation modification spectra, indicating that their presence serves as a distinctive marker for differentiating N-acylation from other acylation types. Similar fragmentation patterns were observed using the Alk-C18:0 probe. S/N/O-acylations with Alk-C18:0 acyl chains exhibited the characteristic ion at *m/z* 406.34, and desaturation of Alk-C18:0 to Alk-C18:1 correspondingly shifted the diagnostic ion to *m/z* 404.33 (Figs. 3d and e). Cyclic immonium ions were similarly observed in N-acylation spectra. To validate diagnostic ion efficacy, we employed LDHA as a model protein, identifying modification sites including K5, K81, and K148 with Alk-C16:0 N-acylation, K118 with both Alk-C16:0 and Alk-C18:0 N-acylation, and S161 with Alk-C16:0 O-acylation (Fig. 3f). Manual examination of all modified peptide spectra revealed that, except for K149 which lacked the Alk-C16:0 diagnostic ion (exhibiting only the cyclic immonium ion), all other N-acylation modifications displayed paired diagnostic and cyclic immonium ions, while S161 possessed the Alk-C16:0 diagnostic ion (Fig. S10 in Supporting information). Based on these diagnostic ion discoveries, we established fragmentation patterns for lipidated peptides and identified modification specific diagnostic ions, enhancing confidence in acyl chain heterogeneity assessment resulting from probe intracellular conversion. For N-acylation modifications, diagnostic ions and cyclic immonium ions typically appear in pairs, whereas O-acylation and S-acylation modifications lack cyclic immonium ions, demonstrating that our identification strategy accurately discriminates between modification types. Based on these diagnostic ion discoveries, we established fragmentation patterns for lipidated peptides and identified modification-specific diagnostic ions, enhancing confidence in acyl chain heterogeneity. For N-acylation modifications, diagnostic ions and cyclic immonium ions typically appear in pairs, whereas O-acylation and S-acylation modifications lack cyclic immonium ions, demonstrating that our identification strategy accurately discriminates between modification types.

In our preceding investigations, cleavable bioorthogonal labeling enabled identification of numerous N-acylation and O-acylation modification sites; however, S-acylation site identification remained limited. Despite this technical limitation, S-acylation represents the most prevalent form of protein fatty acylation, with actual abundance significantly exceeding that of N-acylation and O-acylation modifications (Figs. 1b and c). Current estimates suggest that S-acylation may affect 10 %–20 % of the human proteome [35]. Therefore, optimizing existing identification strategies to address the insufficient detection efficiency of S-acylation sites is critically important. To address this challenge, we developed a dual-identification strategy combining hydroxylamine mediated selective hydrolysis and thiol specific blocking with cleavable bioorthogonal labeling, substantially enhancing S-acylation site identification. Specifically, cleavable bioorthogonal labeling alone identified 213 and 137 S-acylation sites using Alk-C16:0 and Alk-C18:0, respectively. Implementation of the dual-identification strategy increased modification site identification by 276 % and 492 %, respectively. Using this enhanced approach with the Alk-C16:0 probe, we identified 1310 total fatty acylation sites, comprising 588 S-acylation sites, 473 N-acylation sites, and 249 O-acylation sites (Figs. 4a and b, Tables S6 and S7 in Supporting information). The Alk-C18:0 probe yielded 1131 fatty acylation sites, including 674 S-acylation sites, 263 N-acylation sites, and 194 O-acylation sites.

We subsequently compared our identified S-acylation sites against the established palmitoylation database SwissPalm [36]. Comparative analysis revealed that our dual-identification strategy discovered 441 and 536 novel S-acylation sites using Alk-C16:0 and Alk-C18:0 probes, respectively (Fig. 4c). Both strategies demonstrated the capability to identify known S-acylation sites, with Strategy 1 showing superior coverage of previously reported sites.

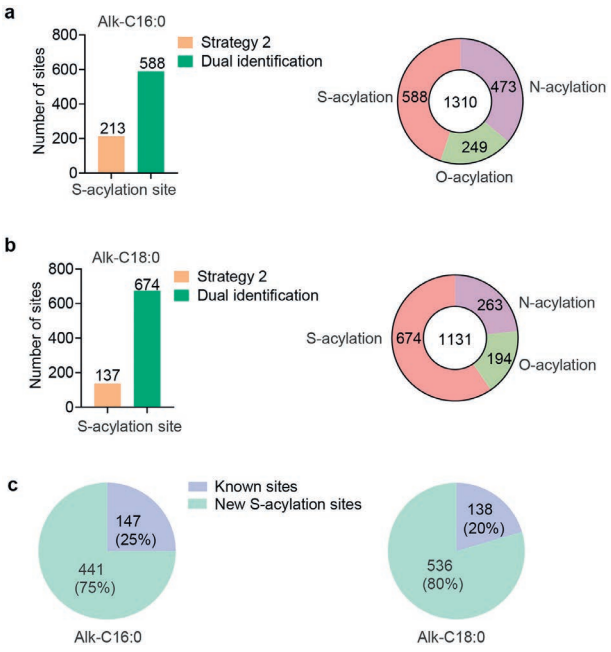


Fig. 4. Dual-identification strategy for global profiling of Alk-C16:0 and Alk-C18:0 lipid acylation modification sites. (a, b) Quantification of acylation sites identified using two probes *via* the dual-identification strategy (FDR = 0.01, Ascore = 20, $n = 3$ independent biological replicates). The final dataset was generated by combining the union of sites identified in any of the three replicates, followed by removal of sites detected in control samples to maximize coverage. (c) Comparison of S-acylation sites identified by the dual strategy with the SwissPalm database.

The application of a dual identification strategy further enhanced the overlap with known sites (Fig. S11 in Supporting information). Furthermore, a portion of S-acylation sites could be detected by both strategies, including C87 on STOM (Figs. S12 and S13 in Supporting information). These findings demonstrate that the dual-identification strategy effectively addresses the limitations of single method approaches for fatty acylation modification site detection, dramatically increasing identification capacity and establishing a robust foundation for comprehensive investigation of fatty acylation modification biological functions and mechanisms.

Using the dual-identification strategy, Alk-C16:0 and Alk-C18:0 probes identified 379 and 297 lipidated proteins, respectively (Fig. 5a). Among these, 190 proteins were detected by both probes, while 189 proteins were exclusively modified by Alk-C16:0 and 107 proteins by Alk-C18:0 (Fig. 5b). To elucidate functional differences between proteins modified by fatty acids of distinct chain lengths, we performed Gene Ontology (GO) enrichment analysis. cellular component analysis revealed that proteins modified by both probes predominantly localize to exosomes, cell membranes, and plasma membranes, suggesting critical roles for fatty acylation in membrane-associated subcellular localization and secretory processes. Notably, Alk-C16:0-modified proteins exhibited significant enrichment in focal adhesion and cytosolic large ribosomal subunit components, whereas Alk-C18:0-modified proteins were enriched in extracellular matrix components, indicating potential involvement in extracellular environment remodeling or signal transduction (Fig. 5c). Biological process analysis demonstrated highly similar functional profiles for both probe-modified proteins, with significant enrichment in translation initiation, viral transcription, and SRP-dependent cotranslational protein targeting to membrane pathways (Figs. 5d and e). These findings indicate that fatty acid modifications of varying chain lengths play pivotal roles in membrane-associated functions and cellular secretory mechanisms through regulation of protein subcellular localization

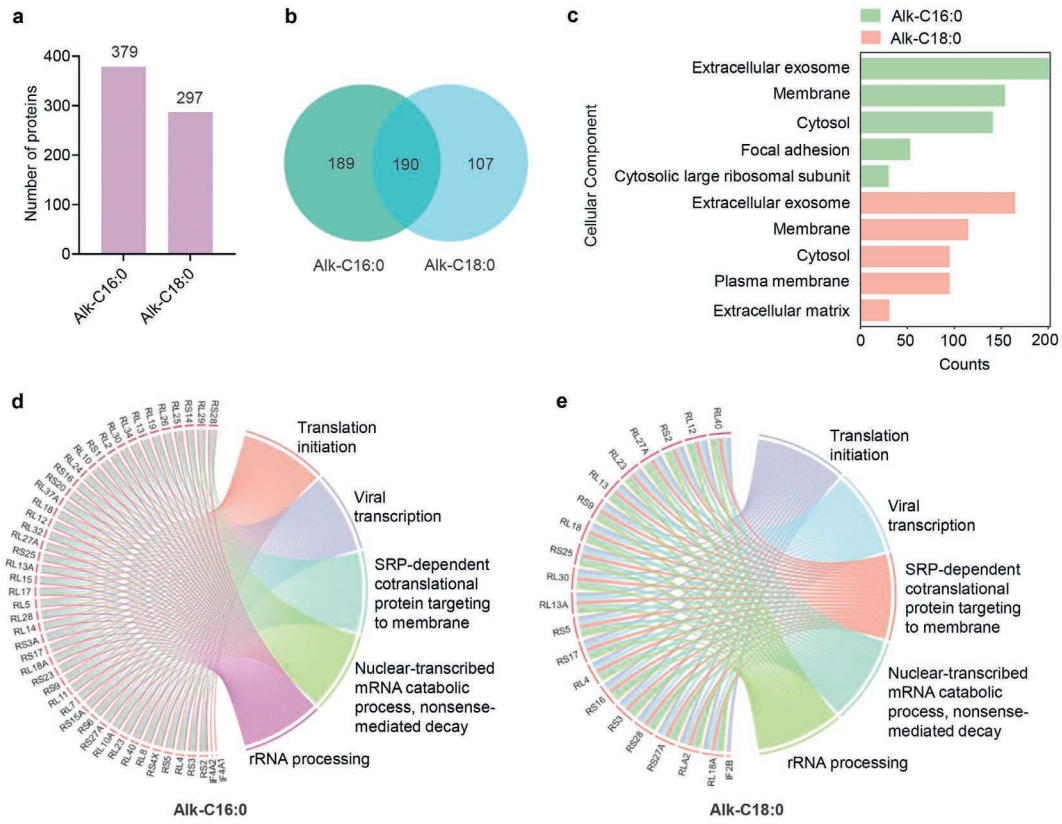


Fig. 5. Functional characterization of proteins modified by Alk-C16:0 and Alk-C18:0. (a) Quantification of fatty acid probe-modified proteins. (b) Comparative analysis of protein sets modified by the two fatty acid probes. (c) GO enrichment analysis of cellular components for lipidated proteins identified with Alk-C16:0 and Alk-C18:0; the top five terms for each probe are shown, ranked by adjusted *P*-values calculated using the Benjamini–Hochberg method. GO enrichment analysis of biological processes for lipidated proteins identified with (d) Alk-C16:0 and (e) Alk-C18:0. The top five terms for each probe are shown, ranked by adjusted *P*-values calculated using the Benjamini–Hochberg method.

and membrane-targeting processes. This work provides crucial insights for comprehensive investigation of fatty acylation modification molecular mechanisms and their functional roles in cellular processes.

Here, we established a dual-identification strategy integrating click chemistry based metabolic labeling with cleavable bioorthogonal tagging and hydroxylamine mediated selective hydrolysis approaches, enabling comprehensive and efficient identification of S-acylation, N-acylation, and O-acylation modifications. This dual strategy overcomes critical limitations including acyl chain information loss and insufficient S-acylation site identification depth. Using Alk-C16:0 and Alk-C18:0 probes, we identified 1310 and 1131 S-acylation sites, respectively, including many previously unreported sites, highlighting the strategy's high efficiency. Through an integrated data analysis pipeline combining open and closed searches, we revealed acyl chain heterogeneity arising from fatty acid probe conversion, providing crucial insights for precise fatty acylation modification identification. Discovery of diagnostic ions further enhanced identification confidence, while identification of cyclic immonium ions significantly improved discrimination between modification types. Integrating these characteristic ions into future database search strategies will increase the depth and accuracy of fatty acylation site identification. Gene Ontology analysis revealed that Alk-C16:0 and Alk-C18:0 modified proteins play essential roles in membrane-associated functions, cell adhesion, protein synthesis, and extracellular matrix remodeling. Collectively, the dual-identification strategy presented in this study provides a robust technological platform for comprehensive fatty acylation analysis, establishing a solid foundation for in-depth investigation of molecular mechanisms and biological functions underlying these modifications.

CRediT authorship contribution statement

Pengfei Wu: Writing – original draft, Investigation, Conceptualization. **Chang Sun:** Investigation. **Xiao Huang:** Investigation. **Wenjing Nie:** Formal analysis. **Qiongqiong Wan:** Formal analysis. **Qingtao Meng:** Formal analysis. **Suming Chen:** Writing – review & editing, Supervision, Funding acquisition, Conceptualization.

Declaration of competing interest

The authors declare that they have no known competing financial interests or personal relationships that could have appeared to influence the work reported in this paper.

Acknowledgments

This work was financially supported by the Noncommunicable Chronic Diseases-National Science and Technology Major Project (No. 2024ZD0532100) and the National Natural Science Foundation of China (No. 22474098).

Supplementary materials

Supplementary material associated with this article can be found, in the online version, at doi:10.1016/j.cclet.2026.112530.

References

[1] B. Chen, Y. Sun, J. Niu, et al., Cell Chem. Biol. 25 (2018) 817–831.
[2] H. Jiang, X. Zhang, X. Chen, et al., Chem. Rev. 118 (2018) 919–988.
[3] J.J. Chen, Y. Fan, D. Boehning, Front. Mol. Biosci. 8 (2021) 656440.
[4] Q. Wan, Y. Xiao, G. Feng, et al., Chin. Chem. Lett. 35 (2023) 108775.
[5] L.H. Chamberlain, M.J. Shipston, Physiol. Rev. 95 (2015) 341–376.
[6] G.P.H. Ho, E.C. Wilkie, A.J. White, et al., Sci. Signal. 16 (2023) eadd7220.
[7] Y. Chang, J. Zhu, X. Li, et al., Signal Transduct. Target Ther. 9 (2024) 254.
[8] Y. Mo, Y. Han, Y. Chen, et al., Mol. Cancer 23 (2024) 274.
[9] L. Zhou, G. Lian, T. Zhou, et al., Nat. Cancer 6 (2025) 768–785.
[10] E. Thinon, J.P. Fernandez, H. Molina, et al., J. Proteome Res. 17 (2018) 1907–1922.
[11] M.D. Resh, Prog. Lipid Res. 63 (2016) 120–131.
[12] R. Takada, Y. Satomi, T. Kurata, et al., Dev. Cell 11 (2006) 791–801.
[13] C. Zou, B.M. Ellis, R.M. Smith, et al., J. Biol. Chem. 286 (2011) 28019–28025.
[14] X. Liang, Y. Lu, T.A. Neubert, et al., J. Biol. Chem. 277 (2002) 33032–33040.
[15] M.T. Forrester, D.T. Hess, J.W. Thompson, et al., J. Lipid Res. 52 (2011) 393–398.
[16] G. Ji, R. Wu, L. Zhang, et al., Anal. Chem. 95 (2023) 13055–13063.
[17] J. Zhang, H. Peng, Z.a. Chen, et al., Chin. Chem. Lett. 35 (2024) 108560.
[18] J. Lin, X.D. Li, Chin. Chem. Lett. 29 (2018) 1051–1057.
[19] B.R. Martin, B.F. Cravatt, Nat. Methods 6 (2009) 135–138.
[20] C.A. Ocasio, M.P. Baggelaar, J. Sipthorp, et al., Nat. Biotechnol. 42 (2024) 1548–1558.
[21] W. Tiantian, Z. Yu, Z. Hao, et al., Chin. Chem. Lett. 34 (2023) 107887.
[22] R. Wu, G. Ji, W. Chen, et al., Analyst 149 (2024) 1111–1120.
[23] J. Luo, Q. Wan, S. Chen, Chin. Chem. Lett. 36 (2025) 109836.
[24] L. Xue, D.R. Gollapalli, P. Maiti, et al., Cell 117 (2004) 761–771.
[25] Y. Ji, N. Leymarie, D.J. Haeussler, et al., Anal. Chem. 85 (2013) 11952–11959.
[26] J. Szychowski, A. Mahdavi, J.J. Hodas, et al., J. Am. Chem. Soc. 132 (2010) 18351–18360.
[27] J.-X. He, Z.-C. Fei, L. Fu, et al., Nat. Chem. Biol. 18 (2022) 904–912.
[28] N.H. Tran, R. Qiao, L. Xin, et al., Nat. Methods 16 (2019) 63–66.
[29] J. Greaves, K.R. Munro, S.C. Davidson, et al., Proc. Natl. Acad. Sci. U. S. A. 114 (2017) E1365–E1374.
[30] D.P. Zolg, M. Wilhelm, T. Schmidt, et al., Mol. Cell. Proteomics 17 (2018) 1850–1863.
[31] N. Wan, N. Wang, S. Yu, et al., Nat. Methods 19 (2022) 854–864.
[32] Q. Wan, Z. Zhang, M. Zhao, et al., Chin. Chem. Lett. 36 (2025) 110794.
[33] M.B. Trelle, O.N. Jensen, Anal. Chem. 80 (2008) 3422–3430.
[34] D. Liu, W. Xiao, H. Li, et al., J. Am. Chem. Soc. 145 (2023) 12673–12681.
[35] S.F. Mesquita, L. Abrami, M.E. Linder, et al., Nat. Rev. Mol. Cell Biol. 25 (2024) 488–509.
[36] M. Blanc, F.P.A. David, F.G. van der Goot, Methods Mol. Biol. 2009 (2019) 203–214.